In press, NeuroImage, August 11, 2015

Simultaneous head tissue conductivity and EEG source location estimation

Zeynep Akalin Acar[*,a,1], Can E. Acar[1,2], Scott Makeig[a,3]

[a] *Swartz Center for Computational Neuroscience, Institute for Neural Computation, University of California, San Diego, La Jolla CA 92093-0559*
[b] *Qualcomm Technologies, Inc. 5775 Morehouse Drive, San Diego, CA 92121*

Abstract

Accurate electroencephalographic (EEG) source localization requires an electrical head model incorporating accurate geometries and conductivity values for the major head tissues. While consistent conductivity values have been reported for scalp, brain, and cerebrospinal fluid, measured brain-to-skull conductivity ratio (BSCR) estimates have varied between 8 and 80, likely reflecting both inter-subject and measurement method differences. In simulations, mis-estimation of skull conductivity can produce source localization errors as large as 3 cm. Here, we describe an iterative gradient-based approach to Simultaneous tissue Conductivity And source Location Estimation (SCALE). The scalp projection maps used by SCALE are obtained from near-dipolar effective EEG sources found by adequate independent component analysis (ICA) decomposition of sufficient high-density EEG data. We applied SCALE to simulated scalp projections of 15 cm^2-scale cortical patch sources in an MR image-based electrical head model with simulated BSCR of 30. Initialized either with a BSCR of 80 or 20, SCALE estimated BSCR as 32.6. In Adaptive Mixture ICA (AMICA) decompositions of (45-min, 128-channel) EEG data from two young adults we identified sets of 13 independent components having near-dipolar scalp maps compatible with a

[*]Corresponding Author
Email addresses: zeynep@sccn.ucsd.edu (Zeynep Akalin Acar), canacar@canacar.net (Can E. Acar), smakeig@ucsd.edu (Scott Makeig)

[1]Designed research, performed research, contributed analytic tools, analyzed data, wrote the paper

[2]Contributed analytic tools.

[3]Designed research, analyzed data, wrote the paper.

single cortical source patch. Again initialized with either BSCR 80 or 25, SCALE gave BSCR estimates of 34 and 54 for the two subjects respectively. The ability to accurately estimate skull conductivity non-invasively from any well-recorded EEG data in combination with a stable and non-invasively acquired MR imaging-derived electrical head model could remove a critical barrier to using EEG as a sub-cm^2-scale accurate 3-D functional cortical imaging modality.

Key words: EEG, source localization, skull conductivity estimation, Finite Element Method, FEM, four-layer realistic head modeling, sensitivity of EEG to skull conductivity

---

1. Introduction

Human electroencephalographic (EEG) source localization aims to reconstruct the current source distribution in the brain from one or more maps of potential differences measured noninvasively from electrodes on the scalp surface. An electric forward head model of the head plays a central role in accurate source localization. The volume conduction model must specify both the geometry and the conductivity distribution of the modeled tissue compartments (scalp, skull, cerebrospinal fluid, brain grey and white matter, etc.). While it is possible to extract head geometry information from magnetic resonance (MR) images of the subject's head (Dale et al., 1999; Akalın-Acar and Gençer, 2004; Ramon et al., 2006), there has been no effective way to directly and non-invasively measure brain and skull tissue conductivities (Ferree et al., 2000; Goncalves et al., 2003b). Studies involving direct skull measurements have reported consistent conductivity values for scalp, brain, and cerebrospinal fluid (CSF). However, skull and therefore brain-to-skull conductivity ratio (BSCR) values reported in the literature (detailed below) have varied between 8 and 80 in adults (Hoekema et al., 2003; Rush and Driscoll, 1968). This presents a problem for accurate EEG source localization, as we have shown in a previous study in which we examined the effects of forward modeling errors on EEG source localization (Akalin Acar and Makeig, 2013).

There, using four-layer BEM head models based on four young-adult MR head images, we estimated the volume-conducted scalp projections of a 3-D grid of equivalent dipole brain sources and then localized the same sources from their projected scalp maps in head models incorporating different BSCR

value assumptions and examined the resulting localization errors. Assuming the simulated BSCR value of 25 in the forward head model allowed near perfect dipole source localization; assuming an (incorrect) BSCR value of 15 gave a maximum error of 15 mm for equivalent dipoles near the skull (grid median, 5 mm), while assuming a BCSR value of 80 gave still larger localization errors up to 31 mm in magnitude (grid median, 12 mm). These localization errors were larger for sources near the skull or brain base; the closer the sources to the center of the brain, the lower the localization error. However, most cortical EEG sources, including those found by independent component analysis (ICA), are relatively near the skull. These simulations demonstrated that the current absence of a method for performing accurate, non-invasive skull conductivity estimation for each EEG subject is a major factor limiting the accuracy of EEG source reconstruction.

1.1. Measuring skull conductivity

Rush and Driscoll (1968) first reported an adult BCSR of 80 by measuring impedances through a half-skull immersed in fluid, thereby establishing a standard still commonly used in inverse source localization software. More recent conductivity estimates have been obtained from combining EEG data with magnetoencephalographic (MEG) and/or invasively recorded electrocorticographic (ECoG) data (Gutierrez et al., 2004; Baysal and Haueisen, 2004; Lai et al., 2005; Lew et al., 2009), or by using current injection or magnetic field induction, an approach termed electrical impedance tomography (EIT) (Ferree et al., 2000; Gao et al., 2005; Ulker Karbeyaz and Gencer, 2003).

A mean BSCR of 72 was reported in a study of six subjects (Goncalves et al., 2003a) based on analysis of evoked somatosensory EEG potentials and MEG fields (SEP/SEF). The same group, however, reported a mean value of 42 using EIT (Goncalves et al., 2003b). Meanwhile, Oostendorp measured BSCR values as low as 15 for a piece of skull temporarily removed during a pre-surgical monitoring study (Oostendorp et al., 2000). Other relatively low BSCR estimates (18.7 ± 2.1) have since been reported for two epilepsy patients from *in vivo* experiments using intracranial electrical stimulation by injecting current using subdural electrodes (Zhang et al., 2006), and BSCR values between 18 and 32 have been derived from simultaneous intracranial and scalp EEG recordings for adult epilepsy patients during pre-surgical evaluations (Lai et al., 2005). Such variations in reported BSCR values may occur not only based on measurement method differences but also through natural

inter-subject variations in skull thickness and density, both also known to change throughout the life cycle (Oostendorp et al., 2000; Hoekema et al., 2003; Wendel et al., 2010).

Considering its strong influence on the accuracy of EEG source localization, skull conductivity should be a subject-specific parameter in any accurate electrical forward head model (Akalin Acar and Makeig, 2013; Huiskamp et al., 1999; Dannhauer et al., 2011). However, as surveyed above most direct skull conductivity measurement methods are invasive. Less invasive methods based on electrical impedance tomography (EIT) or magnetic resonance EIT (MREIT) that inject or induce small currents to estimate conductivity require special equipment and are not in common use. For instance, Ferree *et al* injected small electric currents into scalp EEG electrodes and recorded the resulting potentials at the other electrodes. Skull conductivity was estimated in a four-layer spherical model using a simplex algorithm that minimized error between measured and computed scalp potentials. The mean reported BSCR value was 24 (Ferree et al., 2000). As a large but variable portion of the current injected flows through the scalp itself, such procedures may also be subject to error or bias.

Other groups have proposed estimating skull conductivity using somatosensory event-related potential (SEP) and evoked field (SEF) peak scalp maps. Gutierrez et al. (2004) used SEP and SEF peak scalp maps to estimate layer conductivities in a four-layer spherical head model, estimating the location iteratively so as to minimize differences in equivalent source locations computed from the MEG and EEG maps. Similarly, Baysal and Haueisen (2004) reported a mean BSCR value of 23 across nine subjects by combining SEP/SEF peak scalp maps. Vallaghe et al. (2007) used an average evoked response in a somatosensory experiment and assumed the source projection to the scalp montage could be modeled by a single equivalent dipole located in the cortex. They estimated BSCR as 81 and 89 for right and left hand SEP. Huang et al. (2007) confirmed that simultaneous EEG and MEG recordings could obtain more accurate source localization than either EEG or MEG recordings alone. They performed a two-step approach, estimating tangential source projections of event-related fields (ERFs), fitting conductivity values, then solving for the radial projections absent in MEG using the simultaneously recorded event-related potentials (ERPs). However, MEG recording is much more expensive and much less commonly available than EEG.

Later, Lew et al. (2009) used simulated annealing (SA) to estimate brain and skull conductivities by pre-computing the forward problem for a set of

brain and skull conductivities and then using an SA optimizer to simultaneously search for the source location and conductivity. They proposed to apply their method to EEG data in which the underlying sources may be unitary and for which very good SNR ratios can be achieved, e.g., at early peaks in auditory and somatosensory evoked response averages. However, estimating conductivities from only one source location could bias the results, whereas using a spatially distributed set of isolated sources might be more accurate and robust.

In the following sections, we first formalize the forward and inverse problems and their solutions, explain the effect of skull conductivity on inverse problem solutions, then illustrate how compactness of the source estimates for near-dipolar source scalp maps depends on skull conductivity. Next, we detail the SCALE ('simultaneous conductivity and location estimation') approach for estimating skull (or other head tissue) conductivity and the location of a number of EEG sources concurrently, describe verification of the SCALE approach in a simulation study, and finally report results of its application to 128-channel EEG data sets from two young adult subjects.

2. Methods

2.1. The EEG forward problem

Let σ be the conductivity distribution of the head and $\bar{J^p}$ be the primary current density representing the brain source(s). Then, the potential distribution ϕ within the head generated by $\bar{J^p}$ can be represented by the quasi-static Maxwell Equation:

$$\nabla.(\sigma\nabla\phi) = \nabla.\bar{J^p} \qquad \text{inside V} \tag{1a}$$

$$\sigma\frac{\delta\phi}{\delta n} = 0 \qquad \text{on S} \tag{1b}$$

where V and S denote the volume and surface of the conductive body, respectively, and $\bar{n}$ is the unit normal on surface S. Here, the natural boundary condition is assumed, i.e., the normal component of the current density on the surface of the conductive body is set to zero. From Equation 1, ϕ can be solved for when σ and $\bar{J^p}$ are specified. This is the forward problem of electrical source imaging.

When realistic head models are employed, the forward problem is solved using a numerical modeling approach such as the Finite Element Method

(FEM), Boundary Element Method (BEM), or Finite Difference Method (FDM) (Akalın-Acar and Gençer, 2004; Gençer and Acar, 2004; Wolters et al., 2002; Vanrumste et al., 2000). For the numerical solutions in this study we used FEM head models built using the transfer matrix approach (Gençer and Acar, 2004).

2.2. The EEG Inverse Problem

The relationship between scalp EEG signals $\mathbf{Y}$ and underlying brain source activities $\mathbf{S}$ can be modeled by a linear system:

$$\mathbf{Y} = \mathbf{LS} + \mathbf{B} \tag{2}$$

where $\mathbf{S}$ is the source matrix, $\mathbf{B}$ is the noise matrix and $\mathbf{L}$ is the lead field matrix relating source strengths to their volume-projected scalp potentials. When we perform ICA decomposition of the EEG data, here using AMICA (Palmer et al., 2007), then

$$\mathbf{Y} = \mathbf{QT} = \sum_{i=1}^{P} \mathbf{Q_i} \mathbf{T_i'} \tag{3}$$

where P is the number of maximally independent component processes (ICs), $\mathbf{Q_i}$ is the spatial projection pattern (scalp map) of the ith IC, and $\mathbf{T_i}$ is its activity time course. If P_n of P ICs can be identified as near-dipolar, the EEG for these P_n ICs can be written as:

$$\mathbf{Y_n} = \mathbf{Q_n T} = \sum_{i=1}^{P_n} \mathbf{Q_i} \mathbf{T_i'} \tag{4}$$

Solving an EEG inverse problem from $\mathbf{Y_n}$ gives an estimate of the spatial distribution of source activity generating the observed independent component scalp map:

$$\hat{\mathbf{S}}_\mathbf{i} = \underset{\mathbf{S}_i}{\operatorname{argmin}} (\mathbf{LS}_i - \mathbf{Q}_i \mathbf{T}_i') \tag{5}$$

$$\hat{\mathbf{S}} = \sum_{i=1}^{P_n} \hat{\mathbf{S}}_\mathbf{i} \tag{6}$$

where $\hat{\mathbf{S}}_i$ is the source of the ith IC. Here we can use any linear source localization method to estimate the source distribution $\hat{\mathbf{S}}_i$ (Baillet et al., 1999; Ramirez and Makeig, 2006; Mosher et al., 1999). Using simulations, we have shown that BSCR can strongly affect the accuracy of source localization (Akalin Acar and Makeig, 2013).

2.3. Head model sensitivity to conductance parameters

The numerical electrical forward head model is comprised of matrices representing the head geometry, the distribution of conductivity values within the head, and the locations of the scalp sensors. By parameterizing the forward model (conductivity values, sensor locations, skull thickness, etc.) we reasoned it should be possible to perform optimal conductivity estimation using a gradient-based or simplex optimization approach while simultaneously improving the inverse problem solutions, in a particular sense, for the given independent IC sources. As described above, any change in conductance parameters assumed for the several head tissue parameters requires computationally expensive computation of the head model and transfer matrices.

Here we focus on optimizing the skull conductivity estimate alone (equivalent to optimizing the BSCR). Our approach is to attempt to find a skull conductivity (or equivalently, BSCR value) that simultaneously maximizes the compactness of the computed spatial source distribution estimates for many or all of an identified group of near-dipolar ICs while minimizing the spatial difference between measured and computed IC distributions using the relative difference measure (RDM) (Meijs et al., 1989).

Our inclusion of source compactness as an objective is motivated by the large preponderance of short-range cortical connections for both excitatory and, especially, for inhibitory neurons. The sparsity of long-range connections makes it difficult or impossible for a broadly distributed source domain to emit a unitary signal across an EEG dataset. Unitary effective sources of scalp EEG should therefore be small emergent domains or patches of coherence cortical field activities. The relative anatomic separation of such patches gives the tendency for the time courses of their separate activities to be relatively independent of one another, possibly excepting a sparse subset of time points at which they may receive common alerts that modulate their activities. ICA exploits their relative independence to learn spatial filters that separate their time courses by in effect learning their separate projection patterns to the scalp electrode montage, as embodied in the IC scalp maps contained in columns of the matrix inverse of the ICA unmixing matrix.

2.4. Linearizing changes in scalp potentials produced by small changes in assumed tissue conductivity

One way to optimize the BSCR estimate involves linearizing the potential change in the neighborhood of the currently estimated set of tissue conductivities (Gençer and Acar, 2004). To linearize the potentials around a con-

ductivity distribution σ_0, we begin by perturbing the conductivity estimates by $\Delta\sigma$ and writing the resulting conductivity vector as

$$\sigma = \sigma_0 + \Delta\sigma \tag{7}$$

The corresponding potential becomes:

$$\Phi = \Phi_0 + \Delta\Phi \tag{8}$$

If we discretize the head model with N mesh nodes and M mesh elements we can express Equation 1 in matrix notation:

$$\mathbf{A}_\sigma \Phi = \mathbf{b} \tag{9}$$

where Φ is an $N \times 1$ vector of unknown source potentials, σ denotes the $M \times 1$ vector of element conductivities, $\mathbf{A}$ is a sparse, symmetric $N \times N$ matrix containing element geometry and conductivity information, and $\mathbf{b}$ is an $N \times 1$ vector of primary current density. Let $\mathbf{D}$ be an $m \times N$ sparse matrix that selects m electrode locations among the N nodes in the FEM mesh, i.e. $\Phi_s = \mathbf{D}\Phi$.

Changes in the scalp potentials:

$$\Delta\Phi_s = -\mathbf{D}\mathbf{A}_{\sigma_0} \left. \frac{\delta \mathbf{A}_\sigma}{\delta \sigma} \right|_{(\sigma=\sigma_0)} \Phi_0 \Delta\sigma \tag{10}$$

$$\Delta\Phi_s = \mathbf{S}_\Phi \Delta\sigma \tag{11}$$

where $\mathbf{S}_\Phi$ is the $m \times M$ sensitivity matrix, and $\Delta\sigma$ is $M \times 1$. See (Gençer and Acar, 2004) for a detailed derivation of the sensitivity matrix .

2.5. The SCALE approach

We propose an iterative method for noninvasively estimating head tissue (in particular, skull) conductivity values and brain source distributions simultaneously using (1) a realistically shaped finite element method (FEM) head model constructed from a subject MR head image and (2) the scalp maps of 10-30 near-dipolar EEG source processes compatible with a single cortical patch source distribution, identified by ICA decomposition of a sufficient amount and quality of high-density EEG data collected in any experimental condition. Because of its demonstrated efficacy (Delorme et al., 2012), we here use adaptive mixture ICA (AMICA) for this purpose (Palmer et al.,

2007, 2006). We generate subject-specific four-layer FEM forward head models using the Neuroelectromagnetic Forward head modeling Toolbox (NFT) (Akalin Acar and Makeig, 2010), then select 10 or more IC sources whose scalp maps are "dipolar", i.e., well accounted by a single equivalent model dipole, compatible with a source distribution consisting of a compact cortical patch (Delorme et al., 2012). Typically, the equivalent dipole source locations of such IC sources found in decompositions of continuously recorded EEG data are widely distributed across cortex.

More formally, we assume that each IC source represents a far-field projection to the electrodes of local cortical field potentials that are fully or partially coherent across a single small cortical domain or patch of unknown size and shape. In large part because of the extreme preponderance of short-range corticocortical connections ($\leq 100\mu$m), wholly so for inhibitory neurons and glia, and the predominance of tight radial thalamocortical loops, both supporting oscillatory local field dynamics, models of cortical field dynamics (Deco et al., 2008) demonstrate the emergence of such patches or islands of cortical local field synchrony likened to "pond ripples" by Freeman (2003) and to recurring (point spread) avalanches by Beggs and Plenz (2004). Thus, brain connectivity both favors the emergence of temporal synchrony within small, connected cortical domains and minimizes temporal synchrony between such domains other than in exceptional locations and circumstances. Because of the common alignment of cortical pyramidal cells perpendicular to the cortical surface, spatially coherent local field activity across such a patch will have a non-negligible far-field projection to the scalp (Baillet et al., 2001; Nunez and Srinivasan, 2006), forming an effective EEG source whose time course may typically be near statistically independent of the time courses of concurrent far-field potentials generated by other, spatially separated cortical source patches.

Net far-field currents projecting from such EEG source areas are each volume-conducted to nearly all of the scalp electrodes. Each electrode channel sums potentials from multiple effective cortical brain as well as several types of non-brain ("artifact") sources. Because the outward (or inward) "rippling" of the phase waves across the cortical surface is fairly slow (1-2 m/s) (Nunez and Srinivasan, 2006) and their expected effective size is relatively small (circa 1 cm or less) (Beggs and Plenz, 2004; Baillet et al., 2001), at the frequencies of most oscillatory EEG processes the net source projections to the scalp should be nearly spatially stationary. For example, at 10 Hz and 1 m/s wave speed, the phase difference between the center and pe-

riphery of an outspreading circular avalanche 1 cm in diameter is only 18 degrees. Under favorable circumstances therefore, ICA decomposition can separate such effective source activities by linearly decomposing recorded multichannel data into maximally temporally distinct (independent) component processes (Makeig et al., 1996, 2002, 2004) many of which are associated with near "dipolar" scalp projection patterns compatible with an origin in cortical field activity that is spatially coherent across a cm^2-scale cortical patch (Delorme et al., 2012).

Though the ICs used to localize the sources are associated with "near-dipolar" scalp projection patterns, SCALE uses a distributed source model rather than an "equivalent dipole" source model. In the presence of measurement and modeling errors, the fitting error represents the sum of multiple errors from different causes, and cannot be directly used to estimate the conductivity (Vallaghe et al., 2007). An equivalent dipole may be localized as deeper or less deep in the head depending on whether the actual skull conductivity is higher or lower than the head model estimate while keeping the model fitting error low. When the source is constrained to be compact and oriented orthogonal to the cortical surface, however, incorrect estimation of skull conductivity cannot be compensated by simply moving the center of the source estimate deeper or less deep within the head volume. For this reason, distributed source localization of an imaged 2-D cortical source space allows successful conductivity estimation.

When the effective source is constrained to be compact and to lie within and orthogonal to the imaged cortical surface, an error in BSCR estimation cannot be compensated by a shift in patch depth, as it can in 3-D distributed source models (Pasqual-Marqui, 1999), or by increase in effective source area as in minimum-norm approaches (Hämäläinen and Ilmoniemi, 1994; Pasqual-Marqui, 1999). A possible exception is the cingulate sulcus; a (small) upward-oriented source estimate there might not win out over a (still smaller) source estimate on the upper cortical surface. But this geometry (parallel cortical surfaces, one below the other) may only exist rarely in cortex, and it is unlikely that one such mis-localized IC would strongly bias the estimated BSCR.

Using multiple, spatially dispersed IC sources simultaneously for conductivity estimation makes it possible to differentially weight results for each source at each iteration based on a "goodness of fit" criterion, e.g. a measure of the spatial compactness of the IC spatial source distributions that we estimate using the "sparse, compact and smooth" (SCS) algorithm of Cao

et al. (2012) (summarized in the Appendix). The objective of the SCALE approach is then to adapt conductivity values in the subject forward head model so as to best maximize the compactness of the estimated cortical IC source distributions while also maximizing the goodness of fit of their modeled scalp channel projections to the selected IC source maps.

SCALE proceeds in successive alternating (minimum error) source localization and (maximum compactness) conductivity estimation steps, each iteration requiring (re)computation of the electrical forward head model lead field matrix. The method is therefore computationally intense, making implementations using parallel processing desirable. However, the FEM head model formulation we use allows us to linearize the forward problem near a conductivity distribution by creating a sensitivity matrix that maps conductivity changes to resulting changes in scalp electrode potentials (Gençer and Acar, 2004). This allows us to use gradient-based optimization, avoiding the need for more global schemes that may require a larger number of head model evaluations.

The sensitivity matrix derived above allows us to obtain forward problem solutions near a given conductivity distribution σ_0 and source distribution Φ_0 without having to recompute the forward problem at each step. This, in turn, allows us to iteratively search for a change in conductivity $\Delta\sigma$ that improves the solution of the forward problem in the sense of reducing the RDM error of the forward solution g_f for the set of ICs:

$$g_f = \min_{\Delta\sigma} \mathrm{RDM}(\Phi_{EEG}, \Phi_\sigma) = \min_{\Delta\sigma} \mathrm{RDM}(\Phi_{EEG}, (\mathbf{S}\Delta\sigma + \Phi_{\sigma_0})) \tag{12}$$

RDM, a robust measure of source distribution accuracy sensitive to changes in both source magnitude and distribution (Meijs et al., 1989), is defined as:

$$\mathrm{RDM}(\Phi_R, \Phi) = \sqrt{\left(\frac{\sum_{i=1}^{m} (\Phi_{R,i} - \Phi_i)^2}{\sum_{i=1}^{m} \Phi_{R,i}^2} \right)} \tag{13}$$

where Φ_R is the reference potential distribution, Φ is the calculated potential distribution, and m is the number of electrodes. We can then iteratively improve the source estimates using the updated conductivity estimates, repeating this process until the solution converges.

The basic SCALE approach is thus:

1. Generate a forward electrical head model and select a starting σ_0 (a vector of L conductivity values).

2. For each iteration $i = 0, 1, 2, ...,$
   (a) Calculate the forward model using the conductivity distribution, σ_i.
   (b) For each IC$_j$, $j = 1, 2, ..., P_n$ where P_n is the number of near-dipolar ICs.
      i. Estimate source distribution s_j (a vector of n source magnitudes) from Φ_{IC_j} (a vector of m electrode potentials for the j^{th} IC).
      ii. Compute the estimated electrode potentials Φ_j at σ_i from s_j.
      iii. Calculate the sensitivity matrix, $\mathbf{S}_j$ (the $m \times L$ sensitivity matrix for source distribution s_j).
      iv. Compute $\Delta\sigma_j = \min_{\Delta\sigma}(\mathrm{RDM}(\Phi_{IC_j}, \mathbf{S}_j\Delta\sigma + \Phi_j))$.
   (c) Compute $\Delta\sigma_i = \sum_{j=1}^{P_n} w_j \Delta\sigma_j$. ($w_j$s may be used to weight the evidence from the different ICs.)
   (d) Update the conductivity distribution, $\sigma_{i+1} = \sigma_i + \Delta\sigma_i$.
3. Stop if $\Delta\sigma \leq \epsilon$.

2.6. Finding the optimum conductance change

The goal of the SCALE approach described above finds a σ that allows optimization of all or most P_n independent component source distributions. Since each IC source j has a separate sensitivity matrix, we have chosen to compute an optimum $\hat{\Delta\sigma_j}$ for each IC. For this purpose, we search for the $\hat{\Delta\sigma_j}$ value that minimizes the RDM. The final $\Delta\sigma$ is then computed as a weighted sum of these values. Using equations (13) and (11):

$$\mathrm{RDM}(\Phi_{IC_j}, \Phi_{j,\sigma+\Delta\sigma}) = \sqrt{\left(\frac{\sum_{i=1}^{m}(\Phi_{IC_j} - \Phi_{j,\sigma+\Delta\sigma})^2}{\sum_{i=1}^{m}\Phi_{IC_j}^2}\right)} \quad (14)$$

$$= \sqrt{\left(\frac{\sum_{i=1}^{m}(\Phi_{IC_j} - \Phi_j - \mathbf{S}_j\Delta\sigma)^2}{\sum_{i=1}^{m}\Phi_{IC_j}^2}\right)} \quad (15)$$

Since the RDM function is non-linear, and the sensitivity matrix is only accurate near σ_0, a straightforward approach is to first scan a coarsely-spaced set of pre-selected BSCR values in a fixed range near σ_0 for a skull conductivity value giving the lowest RDM value. The computation of the new potential

$\Phi_j(\sigma + \Delta\sigma)$ at each $\Delta\sigma$ only requires a multiplication by the sensitivity matrix (Equation 15), making scanning a single-variable conductivity change quite fast compared to the rest of the procedure. However, if the SCALE approach were used to search for more than one tissue conductivity, using a more global optimization algorithm could be preferable.

Following the above steps results in $\Delta\sigma$, an $L \times P_n$ matrix of optimal conductivity values for each IC. The $\hat{\Delta\sigma}$ for each iteration is computed as a weighted sum of the columns of this matrix:

$$\hat{\Delta\sigma} = \Delta\sigma \mathbf{w} \tag{16}$$

We tested three different approaches to choosing the source weight vector $\mathbf{w}$ in Equation 16:

1. M1: Weight every source equally: $w_i = 1/P_n, \qquad i = 1...P_n$
2. M2: Weight the estimate source according to the compactness of its estimated source distribution.

$$w_i = \frac{\text{compactness}(i)}{\sum_{j=1}^{P} \text{compactness}(j)}, \qquad i = 1...P_n$$

3. M3: Incorporate both the compactness and the RDM in computing the source weight:

$$w_i = \frac{\text{compactness}(i) \times \text{RDM}(\Phi_{IC_i}, \Phi_i)}{\sum_{j=1}^{P} \text{compactness}(j) \times \text{RDM}(\Phi_{IC_j}, \Phi_j)}, \qquad i = 1...P_n.$$

In the equations above, compactness(i) is the compactness of the potential distribution estimated for the ith source as follows:

$$\text{compactness} = \frac{1}{T^2} \sum_{i=1}^{T} \sum_{j=1}^{T} \Phi_i \Phi_j e^{k\|r(i) - r(j)\|} \tag{17}$$

where T is the number of voxels in the source distribution whose absolute weight values are above a given threshold, and $r(i) - r(j)$ is the distance between the source voxels. In our calculations we used 0.1 for k as this value produced monotonically increasing compactness values when the BSCR value approached the asymptotic BSCR value in our simulation studies.

2.7. Forward head model and EEG data

To test the SCALE approach using actual EEG data we used two data sets (45 min, 128 scalp channels, 256-Hz sampling rate) collected using a Biosemi Active Two system during an arrow flanker task (McLoughlin et al., 2014) from two male subjects, 20 and 23 years of age. Whole-head T1-weighted MR images with 1-mm^3 voxel resolution for the two subjects obtained using a 3-T GE MRI system were used to generate four-layer realistic head tissue models via the NFT toolbox (Akalin Acar and Makeig, 2010) that models scalp, skull, CSF, and brain tissues. We also generated a high-resolution cortical surface source space containing 80,000 sources for each subject using Freesurfer (Dale et al., 1999). The median surface area of the face of the elements on the source space mesh was 0.8 mm^2. The tissue surface and cortical source space meshes for subject S1, as well as the locations of the 128 scalp electrodes are shown in Figure 1.

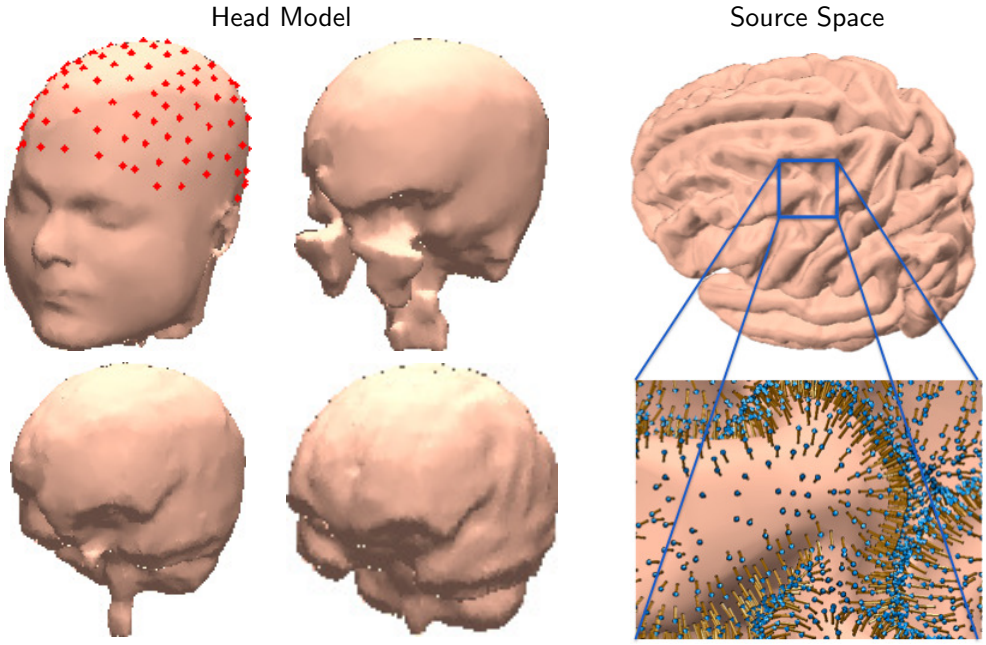

Figure 1: (Left) Scalp, skull, CSF and brain surfaces for subject S1 including the measured 128 scalp electrode locations. (Right) High-resolution Freesurfer cortical source space for subject S1.

For each subject, after high-pass filtering the continuous EEG data above 1 Hz we removed artifacts by initial likelihood-based rejection of time points

(5%-10% of data) (McLoughlin et al., 2014), and applied (single-model) AMICA decomposition (Palmer et al., 2007) and then selected 13 near-dipolar ICs with brain-based equivalent dipoles for Subjects S1 and S2 (Figure 2).

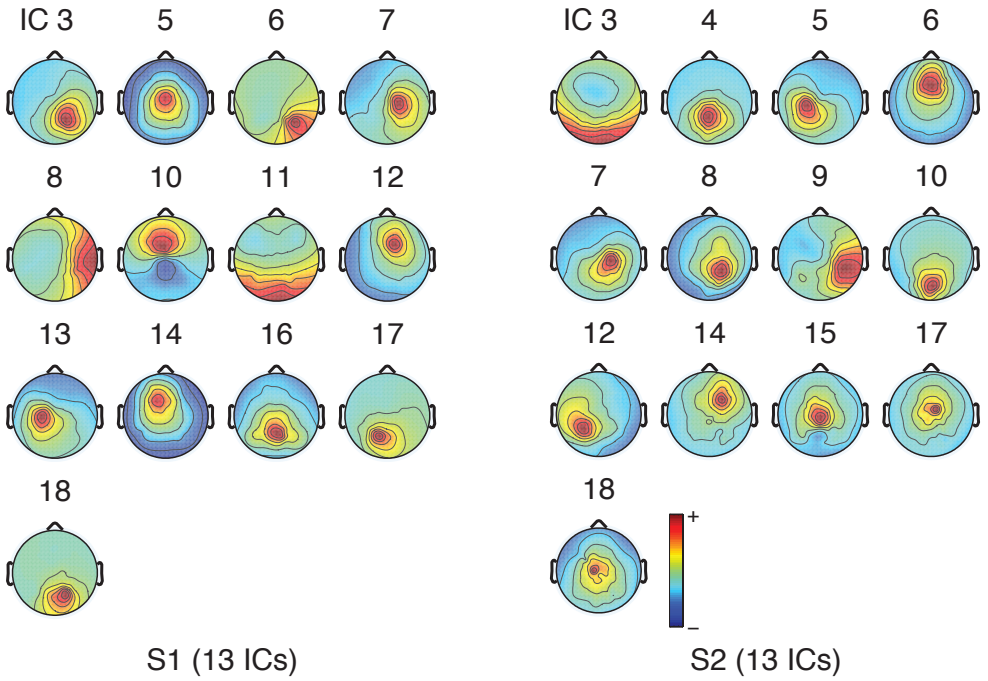

Figure 2: Scalp maps of the near-dipolar brain-based independent component (IC) processes used for subjects S1 and S2.

Our previous simulations using subject-specific BEM head models demonstrated that the overall effect of changing the assumed skull conductance (and thus, BSCR) on recovered dipole source locations is to smoothly and monotonically decrease or increase the depth of the source solutions (Akalin Acar and Makeig, 2013). In those simulations, the source space employed was the homogeneous 3-D brain volume. Here, we used a high-resolution cortical surface source space derived from a subject MR head image using Freesurfer (freesurfer.net) (Fischl, 2012). Thereby, we assumed that the far-field projections of an IC source can be modeled as a weighted sum of a patch of adjacent equivalent dipoles in the cortical mantle whose orientations are orthogonal to the local orientation of the cortical surface (Baillet and Garnero, 1997).

Since the geometry of the oriented cortical source space conforms to the highly invaginated cortical surface, the largest part of whose surface area

is in cortical sulci (fissures) rather than in (outward-facing) gyral surfaces, the effects of changes in the modeled BSCR on distributed compact source estimates for a simulated or actual single-patch source are not smooth and continuous. Rather, as change in the BSCR makes the 3-D equivalent dipole for the source move deeper or more superficial, the maximally compact cortical source distribution in the cortical surface-normal source space may fractionate into multiple non-adjacent patches (often with opposite signs) and then coalesce to another more or less compact solution on another gyrus. This process gives local minima in estimated source compactness as a function of assumed BSCR, one located at the correct BSCR value (in nearly all cases the most compact solution) as well as possible relative minima at other BSCR values.

Because of the presence of these local minima, searching for the optimal skull conductivity using a local optimization algorithm is sensitive to initial conditions (Lew et al., 2009). Our approach seems to avoid becoming trapped in local minima by 1) constraining the inverse problem as much as possible using actual physiological constraints, 2) by simultaneously testing the effects of assumed BSCR on multiple ICs with near-dipolar scalp-maps (and thereby compatible with compact single cortical patch source distributions) and, crucially, 3) by weighting the solution in favor of BSCR values that produce more compact source distributions whose scalp projection patterns are close to the given IC scalp maps. In practice, we observe that source distributions for near-dipolar ICs, when estimated by SCS using wrong (not as simulated) or implausible (not plausibly actual) BSCR values, tend to be more spatially dispersed, while distributions using the correct (simulated) or SCALE-learned BSCR values are dominated by a single compact cortical patch.

2.8. Test data

First, we generated multiple head models for the two test subjects to observe whether and how the compactness of compact source distributions may vary as a function of assumed BSCR. For each subject, we generated nine separate FEM electrical forward-problem head models with linear tetrahedral elements using the NFT toolbox (Akalin Acar and Makeig, 2010), incorporating nine different BSCR values (5, 10, 20, 30, 40, 50, 60, 70, and 80). We then estimated the cortical source distributions for the scalp maps of 13 ICs for each subject using the SCS algorithm applied to each of the nine forward models, and measured the compactness of the estimated cortical

source distributions using Equation 17 above. We also computed the mean compactness across all the simulated sources for each subject.

Next, we simulated 15 circular Gaussian patch sources with radius 10 mm and standard deviation 3.33 mm, including both sulcal and gyral sources uniformly distributed across the cortex in the head model of subject S1, as shown in Figure 3, and computed their forward projections to 128 simulated scalp electrode channels. We used this simulation study to evaluate the relative values of three (M1-3) weighting schemes (see Section 2.6) for estimating skull conductivity.

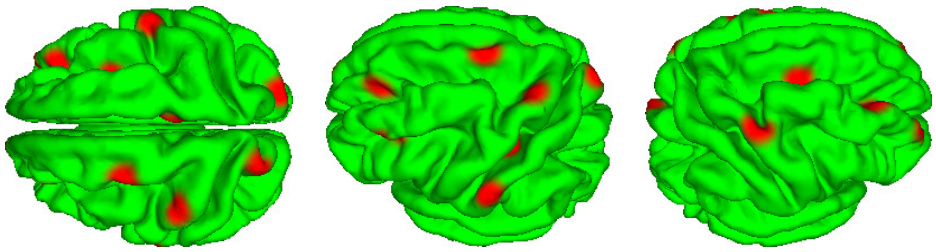

Figure 3: The 15 cortical Gaussian patch sources used in the simulations.

We then computed a reference scalp map projection for each simulated source using a forward-model BSCR of 25 and added sensor noise sufficient to give a signal-to-ratio (SNR) of 20 dB using the definition below (Equation 18). We then estimated skull conductivity with initial BSCR starting values of 80 and 20, using a SCALE approach incorporating each of the three weighing choices to test their relative efficacy.

$$\mathrm{SNR}_{dB} = 10 \log_{10} \left(\frac{\Phi_{EEG}}{\Phi_{noise}} \right)^2 \tag{18}$$

Finally, we applied the iterative SCALE approach to actual EEG data from the two subjects (S1 and S2). For each subject we tested two different starting BSCR values (25 and 80) and also compared the results for the three proposed IC weighing schemes (M1-M3, Section 2.7).

3. Results

Here we report results of three initial tests of the SCALE approach to estimating model head conductance values from EEG data (with scalp channel locations specified) combined with a standard structural MR head image.

3.1. Effects of skull conductivity estimation on source location distributions

The mean source compactness profile for subject S1 (left panel, black trace in Figure 4) was maximum at BSCR = 30, while for subject S2 (right panel), maximum mean source compactness was obtained at BSCR = 60. From this initial test, we concluded that sampling source compactness at discrete BSCR values using may be used to suggest more and less optimal individual subject BSCR values to use in MR head image-derived FEM electrical forward problem head models.

We also explored directly how differences in estimated source distributions for 13 ICs depended on assumed BSCR for the two subjects. Measured source compactness for each IC in each forward model are shown in Figure 4. Estimated source distributions for occipital ICs 16 and 18 had peak compactness at BSCR=30, while source distributions for ICs 7 and 13, with maximum projections to lateral cortex, had highest compactness at BSCR=20. These values fall within the range of values reported in most modern direct BSCR measurement studies. The estimate variation with IC source location and/or orientation could in part reflect regional variations in skull thickness; temporal skull tends to be thinner than occipital skull (Lynnerup, 2001; Anderson, 1882; Hwang et al., 1999).

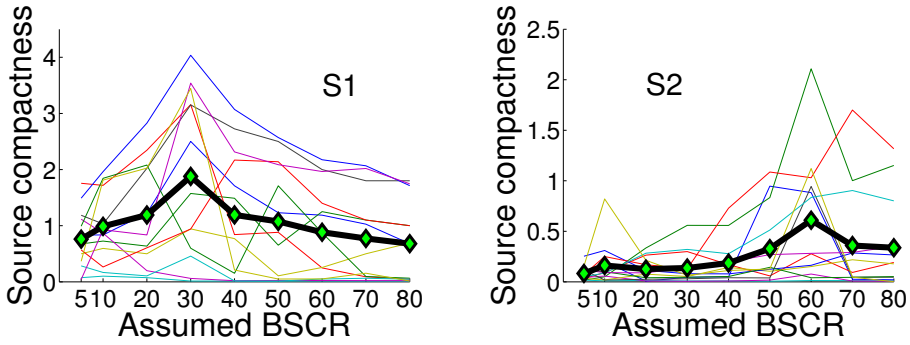

Figure 4: Normalized compactness values for all 13 IC sources (colored traces) using 9 forward head models built from the MR head image for each subject (S1, S2) assuming BSCR estimates from 5 to 80, plus mean compactness for each model (black trace) averaged across all 13 (equally weighted) sources.

3.2. SCALE convergence for simulated EEG patch sources: Effects of IC weighting method

Computing compactness at a set of BSCR values (9 in our initial test above) requires re-computing the FEM matrix for every BSCR value and electrode location. This is a computationally expensive approach, particularly if we wish to seek an exact estimate. To attempt to improve on this blind sampling approach, we tested the application of iterative SCALE estimation by estimating BSCR using a set of 15 simulated single cortical patch-source distributions in the head model of subject S1, attempting to more accurately estimate the simulated BSCR while minimizing the number of the successive BSCR estimates for which the forward head model needs to be recomputed.

We first illustrate source localization results using simulated data in the forward head model of subject S1 for three types of sources; a gyral source, a sulcal source, and a relatively deep interhemispheric source in Figure 5. The data were simulated using BSCR=25. Sensor noise was added to the scalp map (signal-to-noise ratio 20 dB). The simulated source area and the noise-added scalp maps are shown in the upper left corner box in each figure. Source compactness is plotted for BSCR values 5, 10, 20, 30, 40, 50, 60, 70, and 80. Estimated source distributions are visualized at various BSCR values using the semi-inflated cortical surface (sulcal areas in dark grey). In all three cases, the sources are most compact, and compactness values correspondingly maximum, at BSCR test values of 20 or 30.

We then used the SCALE algorithm to estimate skull conductivity with starting BSCR values of 80 and 20, again testing each of the three weighing choices (M1-M3) using simulated IC scalp maps without added noise (Figure 6). We also applied SCALE (using the M3 weighting scheme) to noise-added simulated EEG source scalp maps with signal-to-noise ratios of 20, 25, and 30 dB, again starting SCALE at BSCR=80 and at BSCR=20. We obtained more reliable results using the M3 weighing scheme, likely because it uses both the compactness and model-data goodness-of-fit measures.

In the noise-free case BSCR converged to 32.6, in 17 steps when initialized to 80, and in 9 steps when initialized to 20. When we added noise, the convergence rates were almost the same. For noise-added maps simulated with SNR=30, computed BSCR values converged to 35.2. Thus, given noisy source scalp map data, the BSCR values converged close to the BSCR value (32.6) obtained using noise-free scalp map data with only weak noise-level dependent differences.

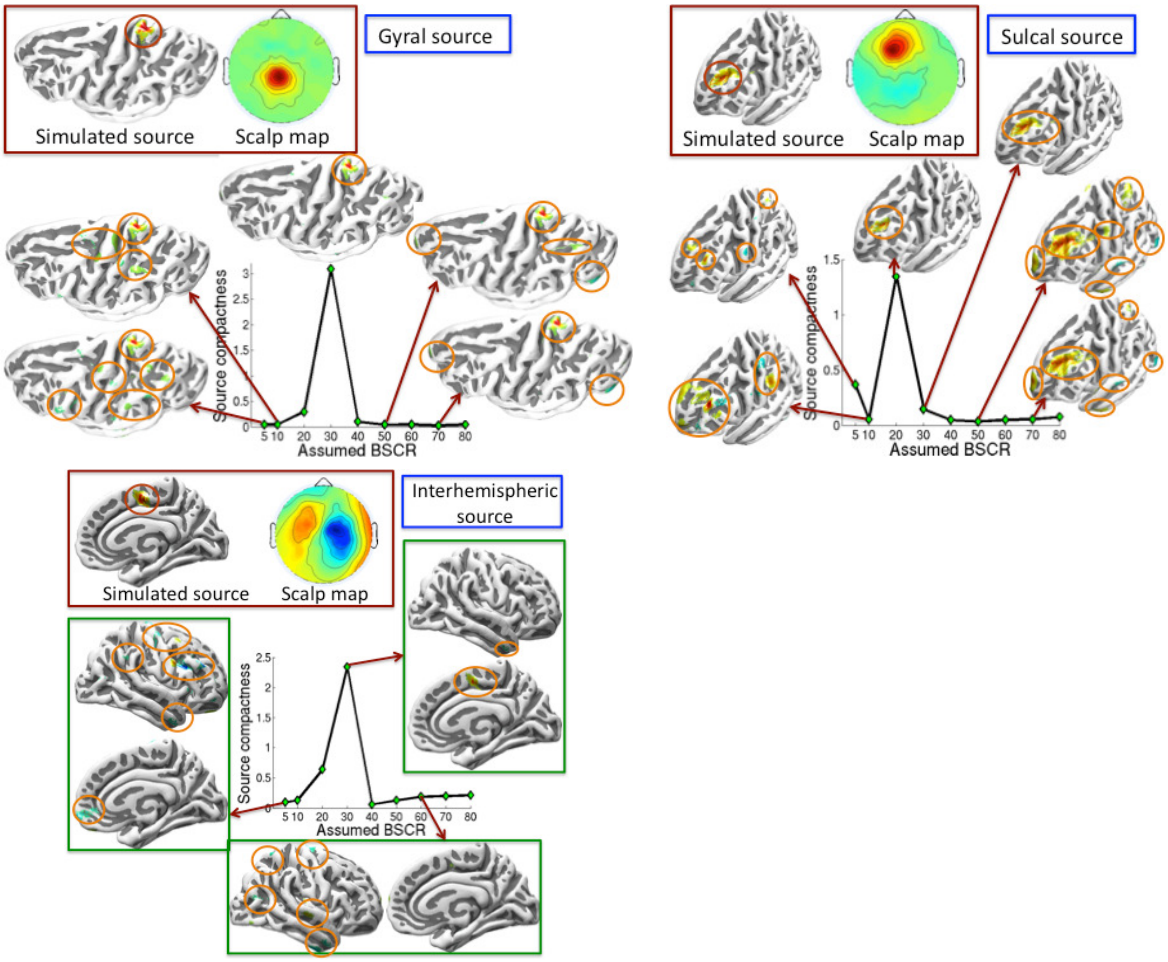

Figure 5: Simulated source localization results using the head model geometry of subject S1 for three sources with noise added; a gyral source, a sulcal source, and a relatively deep interhemispheric source. The simulated source area and the scalp maps (with noise-added) are shown in the upper left corner box in each panel. Source compactness is plotted for BSCR values 5, 10, 20, 30, 40, 50, 60, 70, and 80. Note the strong (rightmost) scalp positivity contributed by the added noise. Estimated source distributions are visualized at some BSCR values on the semi-inflated cortical surface (sulcal areas, dark grey).

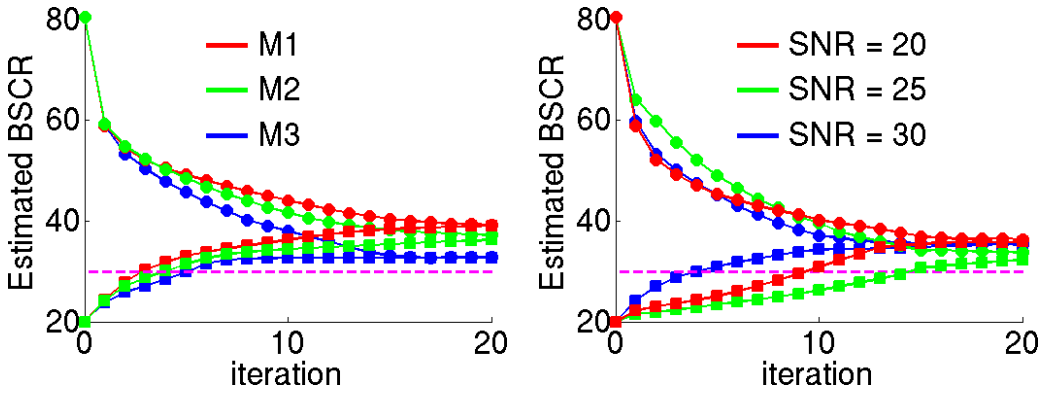

Figure 6: Step-wise convergence of the BSCR estimates produced by SCALE (with M3 weighting) for a simulated data set of 15 cm^2-scale cortical source patches (Figure 3) using a forward head model with a BSCR value of 30. The left figure shows the estimated BSCR value at each step using the source weighting schemes explained in Section 2.6 without adding scalp map noise. The right figure shows the successive BSCR estimates with sensor noise added. The initial SCALE BSCR estimates were BSCR=80 (circular markers) and BSCR=20 (square markers).

3.3. SCALE convergence for actual EEG sources using RDM-based minimization

Finally, we applied the SCALE approach to sets of actual ICs separated by AMICA from the two subjects' recorded EEG data sets. Figure 7 shows the convergence of the BSCR estimates. The M1 (equal) source weighting scheme did not converge, while the M2 and M3 weighting schemes showed similar performance. Therefore only results using M2 and M3 are shown here. For the first subject (left), starting from either initial value (BSCR 80 or 25), SCALE converged to a BSCR estimate of 34 (upper left) while achieving comparable weighted-mean source compactness (near 2.0, lower left). For the second subject (right), again starting at either of the same initial BSCR values SCALE converged to the same estimated BSCR (54) and weighted mean source compactness (near 0.6). The BSCR estimates returned by SCALE (34, 54) remained near the coarse optima (30, 60) dicovered in our initial discrete-value testing (Figure 4).

The BSCR estimates for the two subjects (34, 54) were well separated. *Post hoc* measurements revealed 7.1% more segmented skull voxels in the head model of S2. In the S1 head model, the skull constituted 9.5% of the whole head volume, whereas for S2 the skull constituted 10.2% of the head model. Also, mean skull thickness in S2 was 3.4 mm, whereas for S1 skull

thickness was 3.0 mm. These differences in skull volume and thickness could have contributed to the higher estimated BSCR value for S2 relative to S1. Another possible cause might be higher-density skull compacta layers and/or a thinner skull spongioform layer in S2 (not easily estimated from these MR images).

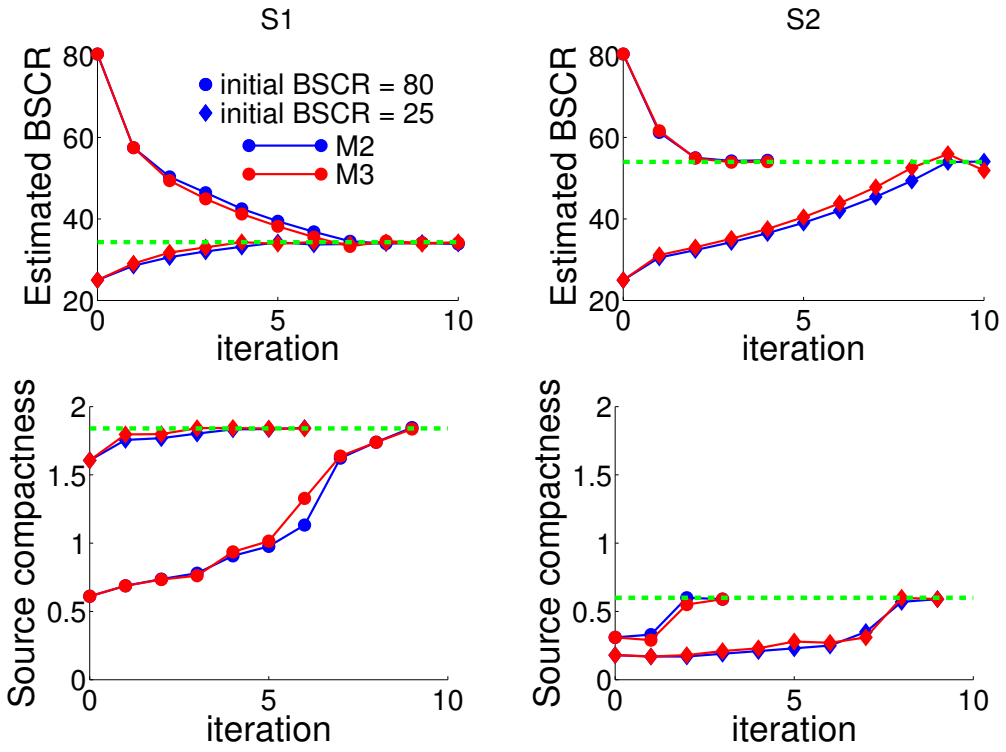

Figure 7: SCALE BSCR value convergence (top row) and weighted-mean estimated source compactness (bottom row) for two sets of 13 brain source-compatible independent sources (ICs) (see Figure 2) separated from actual EEG data of Subjects S1 and S2 respectively using Adaptive Mixture ICA (AMICA). For each subject, SCALE was run beginning with initial BSCR estimates of 80 and 25, respectively, using source weighting schemes M2 and M3.

Figure 8 plots the IC5 source scalp map (top center) and indicates the compactness of the estimated cortical source distribution versus estimated BSCR at each SCALE iteration (red and blue dots), for some iterations estimated source distributions are shown on the semi-inflated cortex model using a (color vs. greyscale) visualization threshold determined by plotting a cumulative histogram (upper left inset) of squared cortical voxel weights

and finding the point of steepest ascent (elbow) of the resulting curve.

Note the changing estimated source area for BSCR estimates near 80 (red dots), becoming more focused on a single cortical patch near convergence. When SCALE iterations begin with a BSCR estimate of 25 (lower left), note the multiple active regions in the source estimate, with strongest activity estimated to be on a different gyrus than in the converged result (upper right). For both starting points, as SCALE iterations progress the active source area converges to nearly the same source distribution (upper right). This example demonstrates how SCALE may be used to stably estimate skull conductivity and thereby to improve the accuracy and robustness of distributed inverse source localization.

3.4. Computational complexity

The computational cost of SCALE depends on head mesh size and on the numbers of sources, electrodes, and modeled conductivity layers. The aim of this section is to indicate how long different stages of the SCALE algorithm require in its present implementation on a single current CPU.

The table below summarizes computation times for a 4-layer realistic head model with a total of 250,000 nodes using a single 2.4-GHz 64-bit Opteron processor. The following parameters define the size of the problem. Typical values for these parameters are also given. N: number of nodes in the FEM mesh ($\sim$ 240,000); L: number of conductivity compartments (1-20); S: number of brain sources (10-30); K: number of source dictionary patches ($\sim$ 80,000); and E: the number of scalp electrodes ($\sim$ 128-256). Based on these parameters, the memory and computation time requirements at various stages of computation as computed and tested (on a $\times$86 64-bit 2600 MHz Linux workstation), respectively:

1. **Forward problem setup:** Generate FEM matrix (N $\times$ N sparse) = 100-200 MB (20 min)
2. **Forward problem solution:** Generate lead field matrix (K $\times$ E full) = 80-160 MB (3.7 hours)
3. **Inverse problem:** Solve $\mathbf{Ax} = \mathbf{b}$ ($\mathbf{A}$=lead field matrix, K $\times$ E; $\mathbf{b}$=scalp potential, E x 1) (1 hour)
4. **Sensitivity matrix:** Generate N $\times$ L $\times$ S full matrix = 20-1,200 MB (6 hours)

Thus, about 11 hours were required to complete the single iteration above. To estimate conductivity while simultaneously refining the source location

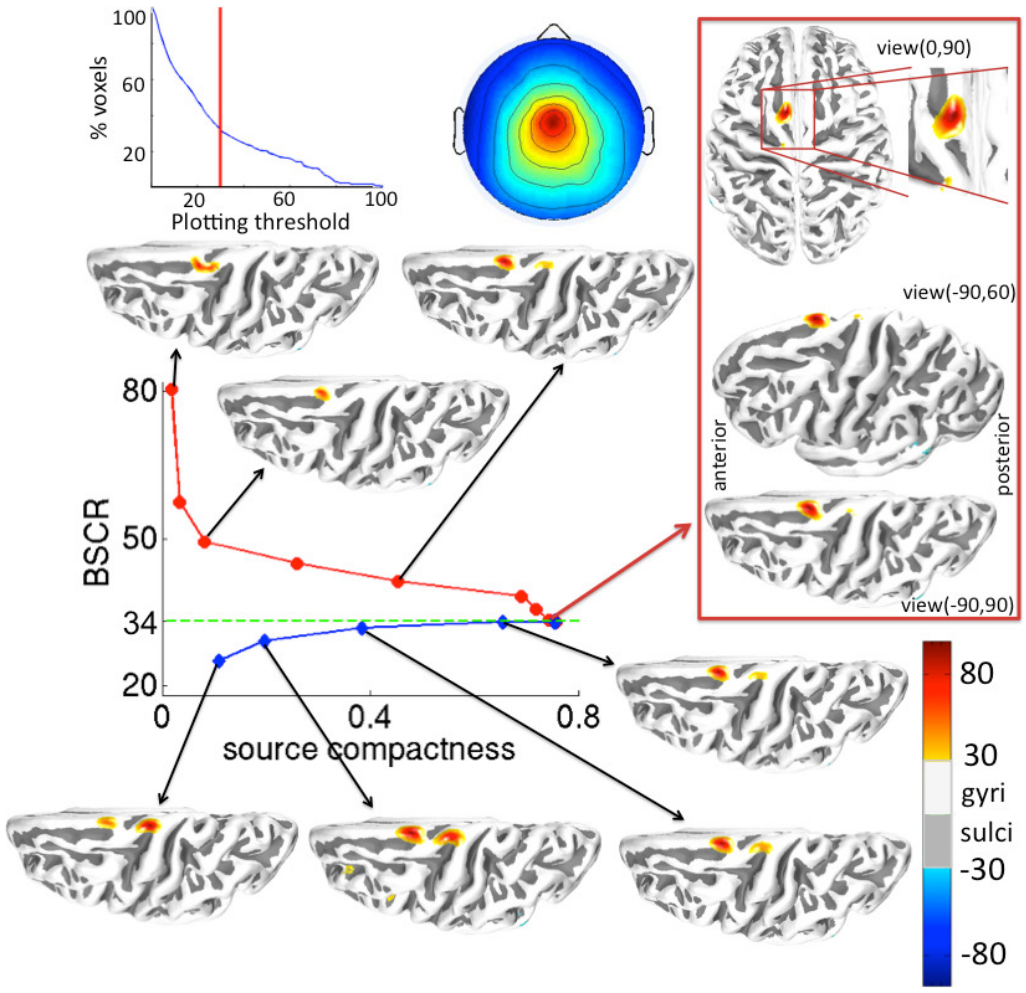

Figure 8: Estimated BSCR, source compactness, and visualized source distributions for IC5 of subject S1 using two SCALE-generated sequences of S1 forward head models for initial estimates BSCR=80 (red trace) and BSCR=25 (blue trace). Semi-inflated cortical surface plots show the estimated (central medial) source distribution at several SCALE iterations. The color bar (lower right) shows estimated voxel source signal density relative to its maximum absolute value. The grey-white to color masking value in these plots ($\pm$30% of the maximum voxel density value) was selected as the elbow in the cumulative histogram (upper left) of squared voxel values in the ultimate source estimate.

estimates, the SCALE algorithm iterated the operations above T = 5-10 times. SCALE thus converged after between 55 and 110 hours (2.3 and 4.6 days) of processing (with N=240,000, K=80,000, E=154, S=13, L=1, T=8).

We anticipate that the most computationally demanding steps above should be straightforward to port to time- and cost-efficient GPU processors. The large number of integral evaluations required to fill in the elements of the sparse FEM matrix can be parallelized. Since the computational intensity (the ratio of mathematical operations to size of input data) for the integral calculations is fairly high, a significant speedup should be achievable (Wolters et al., 2002; Ataseven et al., 2008). In the literature, an 87× speed-up has been reported using a FEM GPU implementation (Fu et al., 2014). A comparable speed-up applied here would reduce the computation time required for a single iteration to only 7.5 minutes, and could give SCALE convergence in 1 hour or less. Further, once learned for a subject, the SCALE-derived forward head model could be used for any data recorded for the same subject, potentially for years afterwards unless head injury or significant skull changes with aging made re-computation necessary. In regular use, only a (highly parallelizable) lead-field matrix computation would be required for each new electrode montage.

4. Discussion

Here we have presented a novel iterative approach (SCALE) to estimating skull conductivity non-invasively from nearly any well-recorded, sufficiently long, high-density EEG data set. SCALE estimates conductivity by simultaneously improving the compactness and stability of distributed EEG source localization for near-dipolar independent component (IC) effective source processes. These ICs are extracted from the data by ICA decomposition and compatible with an origin in a single cortical patch (Delorme et al., 2012). Using the sensitivity matrix in an electrical forward head model built from a subject MR head image, the relationship between changes in implied skull conductivity resulting from changes in scalp potential distribution allow SCALE to iteratively optimize skull conductivity smoothly and efficiently given a number of brain-source compatible source scalp projection maps. SCALE uses overall compactness of the estimated source distributions as a goodness-of-fit criterion.

In our initial tests using distributed simulated source projections, SCALE converged near to the simulated BSCR values. Further, using the final es-

timated (near the simulated) rather than the initially assumed (not as simulated) BSCR values in the SCALE head model gave more accurate source distributions as evidenced by more compact source distributions with lower residual error (Figure 6). Next, we applied SCALE to IC maps derived from two EEG data sets acquired from two young adult male subjects. For both subjects, whether we initialized the BSCR estimate to 80 or to 25 the SCALE result converged to the same BSCR and source distribution estimate, suggesting that the approach successfully avoided falling into local minima.

The final BSCR estimates (34 and 54) were, however, quite different for the two subjects. There might be several reasons for this difference beyond the measured individual difference in skull thickness and volume (Huiskamp, 2008) and other possible skull geometry differences discussed above. Our FEM model only represented four tissue types FEM models including as many as 12 tissue types have been attempted (Ramon et al., 2006). Also, the skull boundaries and cortical surface orientations are not easy to determine precisely from limited-resolution 3-D MRI images (Dogdas et al., 2005; Studholme et al., 1996) and these affect EEG source localization (Lanfer et al., 2012; Ollikainen et al., 1999). These factors may result in geometric and/or electrical head model inaccuracies. In the head modeling used here for SCALE, several approximations are made in forward modeling (Akalin Acar and Makeig, 2010) that may cause skull modeling inaccuracies. For instance, if the FEM model skull layer is somewhat thinner than the subject's skull, then its conductivity should be estimated by SCALE as somewhat higher than its actual value to compensate for this modeling error.

Conductivity is defined as conductance per length (S/m) or equivalently, mS per m of skull depth. For uniform materials, conductance is independent of layer thickness. However, the skull has three layers, two outer compacta layers (reported conductivity 2.25 mS/m) with an intermediate spongiform layer (7.73 mS/m) between them (Akhtari et al., 2000). These authors measured skull layer thicknesses and conductivities in four subjects and found no strong dependence between the thickness of the individual skull layers and their respective conductivities. However, whole skull conductivity does show some dependency. For instance, in a thicker skull in which the thickness of the (higher conductivity) spongiform layer is large relative to the thicknesses of the compacta layers, total skull conductivity can be expected to be higher than that of a thinner skull (Law, 1993). On the other hand, skull conductivity has been shown to be dependent on electrolyte content and on bone density (Akhtari et al., 2000; Chakkalakal et al., 1980). Thus, skull conduc-

tivity may be more strongly dependent on its material properties than on geometric details.

Unlike the simplifying SCALE assumption we used here, skull conductivity is not uniform across its surface. According to Law (1993), radial skull conductivity varies with location and also varies above and near sutures. In Bashar et al. (2010), skull conductivity was measured in 20 different regions, and skull conductivity was reported to vary widely (between 4.7 and 73.5 mS/m). Turovets et al. (2007) segmented a skull into 10-12 anatomically relevant bone plates and, based on parameterized EIT measurements, reported that regional skull conductivity varied between 4 and 44 mS/m while Tang et al. (2008) reported variations between 3.4 and 17.4 mS/m based on *in vivo* measurements of skull fragments. One future improvement to SCALE would be to model the non-uniform conductivity distribution of the skull. Since each source is mainly affected by the conductivity of the skull areas close to the source, different sources individually converge to different conductivity values. Trying to globally optimize the conductivity values of every skull voxel, however, would be a computationally prohibitive and massively ill-posed problem. Estimating a low-dimensional distribution of spatial conductivity differences may, however, prove possible.

In a further exploration Tang et al. (2008) showed that the proportion of spongiform tissue within the skull is positively correlated with its radial conductivity, and confirmed that local skull conductivity may significantly increase near skull sutures. While some researchers have modeled the skull as anisotropic (Marin et al., 1998; Chauveau et al., 2004) or have separately modeled its three layers as isotropic (Sadleir and Argibay, 2007; Dannhauer et al., 2011; Montes-Restrepo et al., 2014), direct modeling of such details may require higher-resolution structural images (e.g., CT images with their imposed radiation risk) and was not attempted here.

While the initial results reported here are promising, SCALE requires further validation using data from more subjects, e.g., including from infants for which at least a few direct measurement results (quite different from those for adults) have been reported. Improving our confidence in the obtained source localizations could also increase confidence in the accuracy of the SCALE approach to EEG source imaging. The validity of its source distribution estimates might be tested using concurrently recorded data from modalities less sensitive to skull conductivity, e.g., conductivities of simultaneously recorded EEG and MEG and/or EEG and ECoG data. One might also test the accuracy of SCALE source localization by including ICs ac-

counting for well-studied features of sensory ERPs in modalities whose most active source locations may possibly be identified in parallel fMRI studies. It may also be of interest to attempt to extend the SCALE approach to learning more conductivity parameters including, e.g., scalp and brain, although correctly estimating skull conductivity should improve source localization more than correctly estimating conductivity for the other head tissue types, as their conductivity ratios are much closer to 1:1 than BSCR values.

The simultaneous conductivity and location estimation (SCALE) approach presented here appears to be a promising non-invasive approach to simultaneously improving skull (and perhaps other brain tissue) conductivity estimates, at the same time improving the accuracy of EEG source distribution estimates based on more optimal single-subject head models. In wider use, the advantage of using individual head models for EEG source imaging might spur the development of low-cost MR head imaging methods. For adults, a forward electrical head model, once computed, might be expected to remain usable for any EEG application until head injury or aging prompted acquisition of a new model. For infants and children, in particular, accurate source localization could for the first time allow accurate measurement of individual consistencies and differences in localized sources of both ongoing and event-related EEG phenomena. Extension of the method to patients with skull insults also seems possible (Akalin Acar et al., 2011). If validated through further study, SCALE might play an important role in advancing the utility and reliability of functional brain imaging using relatively low-cost, wireless, wearable, and easily tolerated, highly temporally-resolved and better spatially-resolved EEG source imaging.

5. Acknowledgements

This work was supported by a grant from the US National Institutes of Health (2R01 NS047293) and by gifts from The Swartz Foundation (Old Field, NY) and an anonymous donor. The authors thank Jason Palmer and Cheng Cao for the AMICA and SCS methods and software used in this work, and Grainne McLoughlin for use of her EEG data. We also thank the anonymous reviewers for their helpful suggestions.

A. The sparse compact and smooth (SCS) EEG inverse problem approach (from (Cao et al., 2012)):

Since the EEG source localization problem is highly under-determined, prior knowledge of the nature of the sources is essential for finding a unique and useful solution. In a Bayesian framework, such knowledge is embedded in the prior distribution $P(\mathbf{d})$. Many existing approaches, such as minimum l_2-norm approaches, minimum current estimation (MCE), SLORETA, etc., often assume that both the dipole strength vector $\mathbf{d}$ and the noise vector $\mathbf{n}$ are normally distributed with zero mean and known covariance matrices Σ_d and Σ_n. These methods encourage source smoothness (Huang et al., 2006; Pasqual-Marqui et al., 2002; Wipf and Nagarajan, 2009; Akalin Acar et al., 2009)). Alternative, sparsity-inducing Bayesian methods such as Sparse Bayesian Learning (SBL) encourage source sparsity (Friston et al., 2008; Wipf and Nagarajan, 2010) learn the form of $P(\mathbf{d})$ from the observed data by updating a set of flexible hyperparameters $\boldsymbol{\gamma}$. The current sources contributing to EEG signals, however, should be *both* spatially compact and locally smooth, typically taking the form of a compact (but non-point like) cortical source patch comprised of parallel dipolar activations aligned with cortical pyramidal cells normal to the cortical surface. This observation led to the development of the Sparse compact smooth (SCS) approach (Cao et al., 2012). A formulation of this approach may be presented using the generalized framework given by Wipf and Nagarajan (2009):

$$P(\mathbf{d}|\mathbf{p}) \propto \exp(-\frac{1}{2}(\mathbf{p}-\mathbf{GD})^{\mathbf{T}}\Sigma_n^{-1}(\mathbf{p}-\mathbf{GD})) \tag{19}$$

$$\Sigma_d = \sum_{i=1}^{d_\gamma} \gamma_i \boldsymbol{C_i} \tag{20}$$

In (20), $\boldsymbol{\gamma} \triangleq [\gamma_1, ..., \gamma_{d_\gamma}]^T$ is a vector of d_γ nonnegative hyperparameters. The appropriate covariance Σ_d can be estimated by modifying γ, whose components control the relative contribution of each covariance basis element $\boldsymbol{C_i}$. The proper hyperparameter $\boldsymbol{\gamma}$ can be estimated by hyperparameter MAP estimation (γ-MAP) Wipf and Nagarajan (2009) which maximizes hyperparameter likelihood $P(\boldsymbol{p}|\boldsymbol{\gamma})$. This is equivalent to minimizing the cost function

$$\boldsymbol{L}(\gamma) = \boldsymbol{p}^{\boldsymbol{T}}\Sigma_p^{-1}\boldsymbol{p} + \log(|\Sigma_p|) \tag{21}$$

where

$$\Sigma_p = \mathbf{G}\Sigma_d\mathbf{G}^{\mathbf{T}} + \Sigma_n \tag{22}$$

After the hyperparameter γ is estimated, yielding the estimated covariance matrix $\widehat{\boldsymbol{\Sigma}}_{\boldsymbol{d}}$ a MAP point estimate of $\boldsymbol{d}$ can be computed

$$\widehat{\boldsymbol{d}} = \widehat{\boldsymbol{\Sigma}}_{\boldsymbol{d}}\boldsymbol{G}^{\boldsymbol{T}}(\boldsymbol{\Sigma}_{\boldsymbol{n}} + \boldsymbol{G}\widehat{\boldsymbol{\Sigma}}_{\boldsymbol{d}}\boldsymbol{G}^{\boldsymbol{T}})^{-\mathbf{1}}\boldsymbol{p} \tag{23}$$

with

$$\widehat{\boldsymbol{\Sigma}}_{\boldsymbol{d}} = \Sigma_i\widehat{\gamma}_i\boldsymbol{C}_i \tag{24}$$

The choice of covariance set $\boldsymbol{C} \triangleq \{C_i : i = 1, ..., d_\gamma\}$ is essential to the solution.

A.1. An alternative model: the SCS algorithm

Instead of modeling the sources as a mixture of multiple Gaussian kernels, Cao et al. (Cao et al., 2012) proposed a correlation-variance model that exploits the fact that one can factor any full-rank covariance matrix into the product of a correlation matrix and the square root of the diagonal variance matrix, as follows:

$$\Sigma_d = \boldsymbol{V}^{\frac{1}{2}}\boldsymbol{R}\boldsymbol{V}^{\frac{1}{2}}, \quad \boldsymbol{V}(i,i) = \sigma^2 \tag{25}$$

The matrix element $\boldsymbol{R}(i,j)$ holds the correlation coefficients between the strengths of the i^{th} and j^{th} dipoles; these values are assumed to be given by a prior estimate. Assuming a local tendency toward synchronization of neural activities at nearby dipoles in the source space, this correlation may be assumed to be exponentially decreasing as the squared distance between dipole locations. A direct definition of the correlation matrix could be

$$R_{ij} = \exp(-a\|\boldsymbol{r}(i) - \boldsymbol{r}(j)\|), \forall i, j = 1, ..., n \tag{26}$$

where $\boldsymbol{r}(i)$ denotes the location of the i^{th} dipole and $\|\boldsymbol{r}(i) - \boldsymbol{r}(j)\|$ is the the Euclidean distance between dipole i and dipole j. However, to guarantee the positive definiteness of the correlation matrix $\boldsymbol{R}$, instead of using the definition in (26) we introduce another matrix $\boldsymbol{H}$ with the same dimension of $\boldsymbol{R}$ such that

$$\boldsymbol{R} = \boldsymbol{H}\boldsymbol{H}^T$$

Here, we assume the that the components of $\boldsymbol{H}$ are given by

$$\boldsymbol{H}(i,j) = \frac{c_i}{1+\exp(a\|\boldsymbol{r}(i)-\boldsymbol{r}(j)\|-b)}, \forall i,j=1,...,n \tag{27}$$

with

$$c_i = \frac{1}{\sqrt{\sum_{i=1}^{n}(1+\exp(a\|\boldsymbol{r}(i)-\boldsymbol{r}(j)\|-b))^2}}, \forall i,j=1,...,n \tag{28}$$

The parameter b is related to the distance within which the correlation coefficient remains at a relatively high level; a is related to the decay rate of the correlation coefficient beyond that distance; c_i is a scaling factor that makes $\boldsymbol{R}(i,i)=1$. The values of a and b can either be pre-defined or learned from the data. After setting proper values for a and b, most entries of $\boldsymbol{H}$ will be close to zero, i.e. $\boldsymbol{H}$ will be a sparse matrix. Therefore, the heavy computational load from the high dimension of H is greatly reduced. In fact, the iteration speed of SCS can be faster than SBL.

The major thrust of the *Sparse, Compact, and Smooth* (SCS) algorithm is to learn from the data the variance of the dipole sources $\boldsymbol{\sigma} \triangleq [\sigma_i,...,\sigma_n]^T$ and $\boldsymbol{\varepsilon} \triangleq [\varepsilon_i,...,\varepsilon_m]^T$, the noise variance under the γ-MAP framework:

$$(\widehat{\boldsymbol{\sigma}},\widehat{\boldsymbol{\varepsilon}}) = \underset{\sigma,\varepsilon}{\operatorname{argmin}} L(\boldsymbol{\sigma},\boldsymbol{\varepsilon}) \tag{29}$$

with

$$\boldsymbol{L}(\boldsymbol{\sigma},\boldsymbol{\varepsilon}) = \boldsymbol{p}^T {\boldsymbol{\Sigma}_{\boldsymbol{p}}}^{-1} \boldsymbol{p} + \log(|\boldsymbol{\Sigma}_{\boldsymbol{p}}|) \tag{30}$$

where $\boldsymbol{\Sigma}_{\boldsymbol{p}}$ is defined as in (22).

We implement the *sparse, compact, and smooth* (SCS) algorithm by using an adaptive gradient approach to updating the *a posteriori* estimate of σ_i and ε_i. This is distinctly different from the way the EM algorithm is used in SBL-based approaches. Here, it avoids computational difficulty due to the non-diagonal structure of Σ_d. Further details of the optimization as well as first sample results can be found in (Cao et al., 2012).

References

Akalın-Acar, Z., Gençer, N. G., 2004. An advanced boundary element method (BEM) implementation for the forward problem of electromagnetic source imaging. Physics in Medicine and Biology 49, 5011–5028, available at `http://www.eee.metu.edu.tr/metu-fp/`.

Akalin Acar, Z., Makeig, S., 2010. Neuroelectromagnetic forward head modeling toolbox. J. of Neuroscience Methods 190, 258–270.

Akalin Acar, Z., Makeig, S., 2013. Effects of forward model errors on EEG source localization. Brain Topography 26, 378–396.

Akalin Acar, Z., Palmer, J., Worrell, G., Makeig, S., 2011. Electrocortical source imaging of intracranial EEG data in epilepsy. In: Proc. of IEEE EMBC.

Akalin Acar, Z., Worrell, G., Makeig, S., 2009. Patch-based cortical source localization in epilepsy. In: Proc. of IEEE EMBC.

Akhtari, M., Bryant, H., Mamelak, A., Heller, L., Shih, J., Mandelkern, M., Matlachov, A., Ranken, D., Best, E., Sutherling, W., 2000. Conductivities of three-layer human skull. Brain Topography 13, 29–42.

Anderson, R., 1882. Observation on the thickness of human skull. Dubl J Med Sci 74, 270–280.

Ataseven, Y., Akalin-Acar, Z., Acar, C. E., Gencer, N. G., 2008. Parallel implementation of the accelerated bem approach for emsi of the human brain. Med. Biol. Eng. Comput. 46, 671–679.

Baillet, S., Garnero, L., 1997. A bayesian approach to introducing anatomo-functional priors in the EEG/MEG inverse problem. IEEE Trans. on Biomed. Eng. 44, 374–385.

Baillet, S., Garnero, L., Marin, G., Hugonin, J., 1999. Electromagnetic brain mapping. IEEE Trans. Biomed. Eng. 46, 522–534.

Baillet, S., Mosher, J. C., Leahy, R. M., 2001. Electromagnetic brain mapping. IEEE Signal Proc. Mag. 18, 14–30.

Bashar, M., Li, Y., Wen, P., 2010. Effects of the local skull and spongiosum conductivities on realistic head modeling. In: IEEE/ICME Int. Conf. on Complex Med. Eng. pp. 23–27.

Baysal, U., Haueisen, J., 2004. Use of a priori information in estimating tissue resistivities - application to human data in vivo. Physiological Meas. 25, 737–748.

Beggs, J., Plenz, D., 2004. Neuronal avalanches are diverse and precise activity patterns that are stable for many hours in cortical slice cultures. The J of Neuroscience 24 (22), 5216–5229.

Cao, C., Akalin Acar, Z., Kreutz-Delgado, K., Makeig, S., 2012. A physiologically motivated sparse, compact, and smooth (SCS) approach to EEG source localization. In: 34th Annual International IEEE EMBS Conference, San Diego.

Chakkalakal, D., Johnson, M., Harper, R., Katz, J., 1980. Dielectric properties of fluid-saturated bone. IEEE Biomed. Eng 27, 95–100.

Chauveau, N., Franceries, X., Doyon, B., Rigaud, B., Morucci, J., Celsis, P., 2004. Effects of skull thickness, anisotropy, and inhomogeneity on forward EEG/ERP computations using a spherical three-dimensional resistor mesh model. Human Brain Mapping 21, 86–97.

Dale, A. M., Fischl, B., Sereno, M. I., 1999. Cortical surface-based analysis: 1. segmentation and surface reconstruction. NeuroImage 9, 179–194.

Dannhauer, M., Lanfer, B., Wolters, C. H., Knosche, T., 2011. Modeling of the human skull in EEG source analysis. Human Brain Mapping 32, 1383–1399.

Deco, G., Jirsa, V., Robinson, P. A., Breakspear, M., Friston, K., 2008. The dynamic brain: From spiking neurons to neural masses and cortical fields. PLOS Comp. Biol. 4 (8).

Delorme, A., Palmer, J., Oostenveld, R., Makeig, S., 2012. Independent EEG sources are dipolar. PLOS One.

Dogdas, B., Shattuck, D., Leahy, R., 2005. Segmentation of skull and scalp in 3-d human MRI using mathematical morphology. Human Brain Mapping 26, 273–285.

Ferree, T., Eriksen, K., Tucker, D., 2000. Regional head tissue conductivity estimation for improved EEG analysis. IEEE Trans. Biomed. Eng. 47, 1584–1592.

Fischl, B., 2012. Freesurfer. Neuroimage 62, 774–781.

Freeman, W., 2003. A neurobiological theory of meaning in perception part ii: Spatial patterns of phase in gamma EEGs from primary sensory cortices reveal the dynamics of mesoscopic wave packets. Int J of Bifurcation and chaos 13, 2513–2535.

Friston, K., Harrison, L., Daunizeua, J., Henson, R., Flandin, G., Mattout, J., 2008. Multiple sparse priors for the M/EEG inverse problem. Neuroimage 39 (3), 1104–1120.

Fu, Z., Lewis, J., Kirby, R., Whitaker, R.-T., 2014. Architecting the finite element method pipeline for the gpu. J. of Comp. and Applied Math. 257, 195–211.

Gao, N., Zhu, S., He, B., 2005. Estimation of electrical conductivity distribution within the human head from magnetic flux density measurement. Phys. in Med and Biol. 50, 2675–2687.

Gençer, N. G., Acar, C. E., 2004. Sensitivity of EEG and MEG measurements to tissue conductivity. Physics in Med.and Biol. 49, 701–717.

Goncalves, S., de Munck, J., Jeroen, P., Heethaar, R., da Silva, F., 2003a. In vivo measurement of the brain and skull resistivities using an eit-based method and realistic models for the head. IEEE Trans. Biomed Eng 50, 754–767.

Goncalves, S., de Munck, J., Verbunt, J., Heethaar, R., da Silva, F., 2003b. In vivo measurement of the brain and skull resistivities using an eit-based method and the combined analysis of SEF/SEP data. IEEE Trans. Biomed Eng 50, 1124–1128.

Gutierrez, D., Nehorai, A., Muravchik, C., 2004. Estimating brain conductivities and dipole source signals with EEG arrays. IEEE Trans. on Biomed. Eng. 51, 2113–2122.

Hämäläinen, M. S., Ilmoniemi, R. J., 1994. Interpreting magnetic fields of the brain. Medical and Biol. Eng. and Comp. 32 (1), 35–42.

Hoekema, R., Wieneke, G., Leijten, F., van Veelen, C., van Rijen, P., Huiskamp, G., Ansems, J., van Huffelen, A., 2003. Measurement of the conductivity of skull, temporarily removed during epilepsy surgery. Brain Topography 16 (1), 29–38.

Huang, M., Dale, A., Song, T., Halgren, E., Harrington, D., Podgorny, I., Carnive, J., Lewis, S., Lee, R., 2006. Vector-based spatial-temporal minimum l1-norm solution for MEG. Neuroimage. 31, 1025–1037.

Huang, M.-X., Song, T., Hagler, D., Podgorny, I., Jousmaki, V., Cui, L., Gaa, K., Harrington, D., Dale, A., Lee, R., Elman, J., Halgren, E., 2007. A novel integrated MEG and EEG analysis method for dipolar sources. Neuroimage 37, 731–748.

Huiskamp, G., 2008. Interindividual variability of skull conductivity: an EEG-MEG analysis. Int. J. of Bioelectromagnetism 10, 25–30.

Huiskamp, G., Vroeijenstijn, M., Van Dijk, R., Wieneke, G., Van Huffelen, A. C., 1999. The need for correct realistic geometry in the inverse EEG problem. IEEE Trans. Biomed. Eng. 46, 1281–1287.

Hwang, K., Kim, J., Baik, S., 1999. The thickness of the skull in korean adults. J of Crabiofacial Surgery.

Lai, Y., van Drongelen, W., Ding, L., Hecox, K., Towle, V., Frim, D., He, B., 2005. Estimation of in vivo human brain-to-skull conductivity ratio from simultaneous extra- and intra-cranial electrical potential recordings. Clinical Neurophysiology 116, 456–465.

Lanfer, B., Scherg, M., Dannhauer, M., Knosche, T., Burger, M., Wolters, C., 2012. Influences of skull segmentation inaccuracies on eeg source analysis. Neuroimage 62, 418–431.

Law, S., 1993. Thickness and resistivity variations over the upper surface of the human skull. Brain Topography 6, 99–109.

Lew, S., Wolters, C., Anwander, A., Makeig, S., MacLeod, R., 2009. Improved eeg source analysis using low-resolution conductivity estimation in a four-compartment finite element head model. Human Brain Mapping 30, 2862–2878.

Lynnerup, N., 2001. Cranial thickness in relation to age, sex, and general body build in a danish forensic sample. Forensic science international 117, 45–51.

Makeig, S., Bell, A. J., Jung, T., Sejnowski, T., 1996. Independent component analysis of electroencephalographic data. Vol. 8. MIT Press, Cambridge.

Makeig, S., Debener, S., Onton, J., Delorme, A., 2004. Mining event-related brain dynamics. Trends in Cognitive Sciences 8 (5), 204–210.

Makeig, S., Westerfield, M., Jung, T.-P., Enghoff, S., Townsend, J., Courchesne, E., TJ., S., 2002. Dynamic brain sources of visual evoked responses. Science 295, 690–694.

Marin, G., Guerin, C., Baillet, S., Garnero, L., Meunier, G., 1998. Influence of skull anisotropy for the forward and inverse problem in EEG: Simulation studies using fem on realistic head models. Human Brain Mapping 6, 250–269.

McLoughlin, G., Palmer, J., Rijsdijk, F., Makeig, S., 2014. Genetic overlap between evoked frontocentral theta-band phase variability, reaction time variability, and attention-deficit/hyperactivity disorder symptoms in a twin study. Biol. Psychiatry 75, 238–247.

Meijs, J. W. H., Weier, O., Peters, M. J., 1989. On the numerical accuracy of the boundary element method. IEEE Trans. Biomed. Eng. 36, 1038–1049.

Montes-Restrepo, V., van Mierlo, P., Strobbe, G., Staelens, S., Vandenberghe, S., Hallez, H., 2014. Influence of skull modeling approaches on EEG source localization. Brain Topogr. 27, 95–111.

Mosher, J. C., Baillet, S., Leahy, R. M., 1999. EEG source localization and imaging using multiple signal classification approaches. J. of Clin. Neurophysiol. 16, 225–238.

Nunez, P., Srinivasan, R., 2006. Electric Fields of the Brain. Oxford University Press, New York, Oxford.

Ollikainen, J. O., Vauhkonen, M., Karjalainen, P. A., Kaipio, J. P., 1999. Effects of local skull inhomogeneities on EEG source estimation. Med. Eng. Phys. 21, 143–154.

Oostendorp, T., Delbeke, J., Stegeman, D. F., 2000. The conductivity of the human skull: Results of in vivo and in vitro measurements. IEEE Trans. Biomed. Eng. 47, 1487–1492.

Palmer, J. A., Kreutz-Delgado, K., Makeig, S., 2006. Super-gaussian mixture source model for ICA. In: Justinian Rosca, Deniz Erdogmus, J. C. P., Haykin, S. (Eds.), Proceedings of the 6th International Symposium on Independent Component Analysis. Springer.

Palmer, J. A., Kreutz-Delgado, K., Rao, B. D., Makeig, S., 2007. Modeling and estimation of dependent subspaces. In: Proceedings of the 7th International Conference on Independent Component Analysis and Signal Separation.

Pasqual-Marqui, R., 1999. Review of methods for solving the EEG inverse problem. Int. J. Bioelectromagnetism. 1, 75–86.

Pasqual-Marqui, R., Esslen, M., Kochi, K., Lehmann, D., 2002. Functional imaging with low resolution brain electromagnetic tomography (LORETA): a review. Methods and findings in experimental and clin. Pharmacology. 24, 91–95.

Ramirez, R., Makeig, S., 2006. Neuroelectromagnetic source imaging using multiscale geodesic neural bases and sparse bayesian learning. In: Proc. of HBM.

Ramon, C., Schimpf, P., Haueisen, J., 2006. Influence of head models on eeg simulations and inverse source localizations. Biomedical Eng. Online 5.

Rush, S., Driscoll, D. A., 1968. Current distribution in the brain from the surface electrodes. Anesthesia and Analgesia, Current res. 47, 717–723.

Sadleir, R., Argibay, A., 2007. Modeling skull electrical properties. Annals of Biomed. Eng. 35 (10), 1699–1712.

Studholme, C., Hill, D., Hawkes, D., 1996. Automated 3-D registration of MR and CT images of the head. Med Image Anal 1, 163–175.

Tang, C., Fusheng, Y., Cheng, G., Gao, D., Fu, F., Yang, G., Dong, X., 2008. Correlation between structure and resistivity variations of the live human skull. IEEE Trans. on Biomed. Eng. 55, 2286–2292.

Turovets, S., Salman, A., Malony, A., Poolman, P., Davey, c., Tucker, D., 2007. Anatomically constrained conductivity estimation of the human head tissues in vivo: computational procedure and preliminary experiments. IFMBE Proceedings 14, 3854–3857.

Ulker Karbeyaz, B., Gencer, N., 2003. Electrical conductivity imaging via contactless measurements: an experimental study. IEEE Trans. Med. Imag. 22, 627–635.

Vallaghe, S., Clerc, M., Badier, J.-M., 2007. In vivo conductivity estimation using somatosensory evoked potentials and cortical constraint on the source. ISBI, 1036–1039.

Vanrumste, B., Van Hoey, G., Van de Walle, R., D'Havé, M., Lemahieu, I., Boon, P., 2000. Dipole location errors in electroencephalogram source analysis due to volume conductor model errors. Med. Biol. Eng. Comp. 38, 528–534.

Wendel, K., Vaisanen, J., Seemann, G., Hyttinen, J., Malmivuo, J., 2010. The influence of age and skull conductivity on surface and subnormal bipolar EEG leads. Comp. Intellegence and Neuroscience 2010.

Wipf, D., Nagarajan, S., 2009. A unified bayesian framework for MEG/EEG source imaging. NeuroImage 44, 947–966.

Wipf, D., Nagarajan, S., 2010. Iterative reweighted l1 and l2 methods for finding sparse solutions. IEEE. J. Selected Topics In Signal Processing 4 (2), 317–329.

Wolters, C. H., Kuhn, M., Anwander, A., Reitzinger, S., 2002. A parallel algebraic multigrid solver for finite element method based source localization in the human brain. Comput. Visual Sci. 5, 165–177.

Zhang, Y., van Drongelen, W., He, B., 2006. Estimation of in vivo brain-to-skull conductivity ratio in humans. Appl Phys Lett 89.